RSC Advances

ROYAL SOCIETY OF CHEMISTRY

www.rsc.org/advances

RSC Advances

PAPER

Response of zeta potential to local membrane fouling forms in dead-end membrane filtration with yeast suspension

Hui Jia [a, b*], Hongmei Zhang[b], Jie Wang[a, b], Hongwei Zhang[a] and Xinbo Zhang[c]

Received 30th June 2015,
Accepted 00th January 20xx

DOI: 10.1039/x0xx00000x
www.rsc.org/

The zeta potential which responded to local membrane fouling forms with yeast suspension was investigated by monitoring both local flux and local zeta potential. Experiments adopting segmentation and in suit monitoring methods during dead-end hollow membrane filtration process were conducted. Comparing the model with experimental data, it could be found that zeta potential reflected the forms of local membrane fouling. The variations in zeta potential during membrane filtration performed differently in pore blocking, cake formation and cake compression processes. When zeta potential decreased rapidly, pore blocking occurred. As zeta potential dropped gradually and linearly, it came to cake filtration. Subsequently, when zeta potential became almost stable, it was experiencing cake compression. Besides, the effect of fiber length on local fouling behavior was also studied. With the increase of fiber length, the time taken by three segments to enter the cake layer compression stage was extended and the difference values of zeta potential in three segments tended to increase.

1. Introduction

Membrane application in water treatment provides many advantages over conventional treatment processes. However, membrane fouling is an inevitable problem impairing all membrane processes, as it leads to reduced permeate flux, increased energy demand, higher maintenance costs, and decreased membrane lifetime, which restricts their widespread applications.[1,2]

Membrane fouling is generally observed as the flux decline during membrane filtration. Fouling phenomenon could be evaluated by analyzing the experimental flux decline data and filtration models.[3,4] The flux decline in dead-end filtration can be explained by classical fouling models including pore constriction (standard blocking)[5], complete pore blockage, intermediate pore blockage[6], cake formation[7] and some combined models which integrated two or more.[8,9] It is very simple to understand membrane fouling mechanism using the above models to analyze flux data, but the actual membrane fouling process is more complicated than that defined according to the hypotheses of these models. In order to understand membrane fouling in-depthly, some online monitoring methods with flux decline measurement have been proposed, such as optical image[10], ultrasonic time domain reflectometry[11,12], cake layer thickness[13], surface charge character.[14,15] Particle deposition can be clearly observed by optical image techniques but the observation has its limitation, that is, the image is only focused on the membrane surface (flat-sheet membranes) or on the side view of the hollow fiber cross-section (hollow fiber membranes). In addition, it takes high testing cost. Li et al[11,12] used a single hollow fiber membrane inserted into two thin polyurethane (PU) hosepipes, of which the interspaces between the fiber and hosepipe were blocked off with epoxy resin to study local fouling distribution along the fiber. However, there was still a deviation between the measurement results and real operational data acquired in membrane filtration process. It would be necessary to point out that ionic deposition and electrokinetic phenomena were not just the problems for single membrane fiber.

The surface charge condition of membrane which provides useful information about the electrostatic interaction between membrane and foulants is an important parameter in fouling studies. In recent years, several researchers have employed the membrane zeta potential as a key parameter to study the fouling characteristics of different types of membrane. The changes of zeta potential between fouled membrane and clean membrane can be used to monitor membrane fouling.[16] Y. Soffer et al[17] applied a method to study the fouling of polysulfone ultrafiltration membranes with different molecular weight cut off, employing the coupling flux with streaming potential method. It demonstrated that two fouling layers formed on original and fouled membrane had different features. It also showed that a linear relationship between the change of zeta potential from the clean to the fouled membrane and the degree of fouling. Besides, M.S. Chun et al[18] researched the evolution of streaming potential coefficient during BSA suspension filtration. It detected a decrease of the streaming potential coefficient from a positive value to a

[a] State Key Laboratory of Seperation Membranes and Membrane Processes, Tianjin Polytechnic University, Tianjin 300387, China. E-mail: ajiahui@163.com; Fax: +86 022 8395 5668; Tel.: +86 022 8395 5668
[b] School of Environmental and Chemical Engineering, Tianjin Polytechnic University, Tianjin 300387, China
[c] School of Environmental and Municipal Engineering, Tianjin Chengjian University, Tianjin 300384, China

negative one as time went on, which meant that the electrostatic repulsion made the BSA particles exist mainly in the concentration polarization layer instead of being deposited onto the outer surface of the hollow fiber. Furthermore, it found that the time evolution of the streaming potential was closely related to the filtrate flux decline. The same phenomenon had also been found by B. Teychene et al.[16] Z.P. Zhao et al[15] showed that the flux and streaming potential method in examining mechanism of charged membrane fouling was complementary, and could provide more microscopic information, which helped to understand the fouling mechanism between material and membrane. Nevertheless, any of those researches scarcely studied the zeta potential changes of different segmented membrane fibers to further understand the membrane filtration process.

This study employed local zeta potential with local flux to in suit monitor local fouling forms in the horizontal dead-end hollow fiber membrane modules divided into three sections (namely upstream, middle, and downstream) under constant pressure operation. And combined model was adopted to analyze the flux data. The effect of fiber length on local fouling forms was also investigated. It was expected that the formation process of local membrane fouling could be described by the response of zeta potential.

2. Experimental

2.1. Membrane and feed suspension characteristics

Polyvinylidene fluoride (PVDF) hollow fiber membranes (Tianjin Motimo Membrane Technology Co. Ltd., China) with a nominal pore size of 0.22 μm, inside and outside diameter of 0.6 mm and 1.1 mm respectively, were used in this study. Each membrane modules was soaked with deionized water at least 24 h to remove the wetting agent prior to use. The

Fig.1 The zeta potential characterizations of yeast solution and clean membrane in 1.0 mM KCl solution.

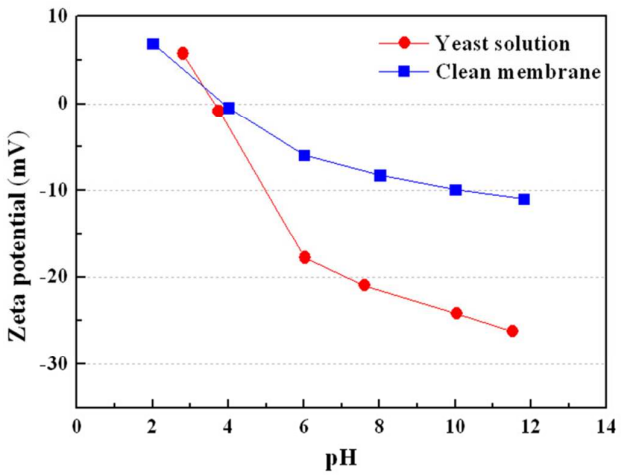

experiments adopted external pressure membrane filtration process.

The fouling experiments were carried out with 0.5 g/L yeast suspension in order to generate appropriate rate of membrane fouling during ultrafiltration experiments. All runs were carried out at room temperature (20±2 °C). Before utilization, active dry yeast (AngelYeast Co. Ltd., China) cells were washed three times with deionized water, centrifuged and dried at 80 °C for 24 h in a hot air oven to deactivate the cells[19], then suspended in distilled water. After processing, their mean diameter is 5.4 μm. The particle size was tested with a laser scattering particle size distribution instrument (Mastersizer 2000, Malvern, UK). The solution was appropriate for the performance analysis of the membrane filtration.

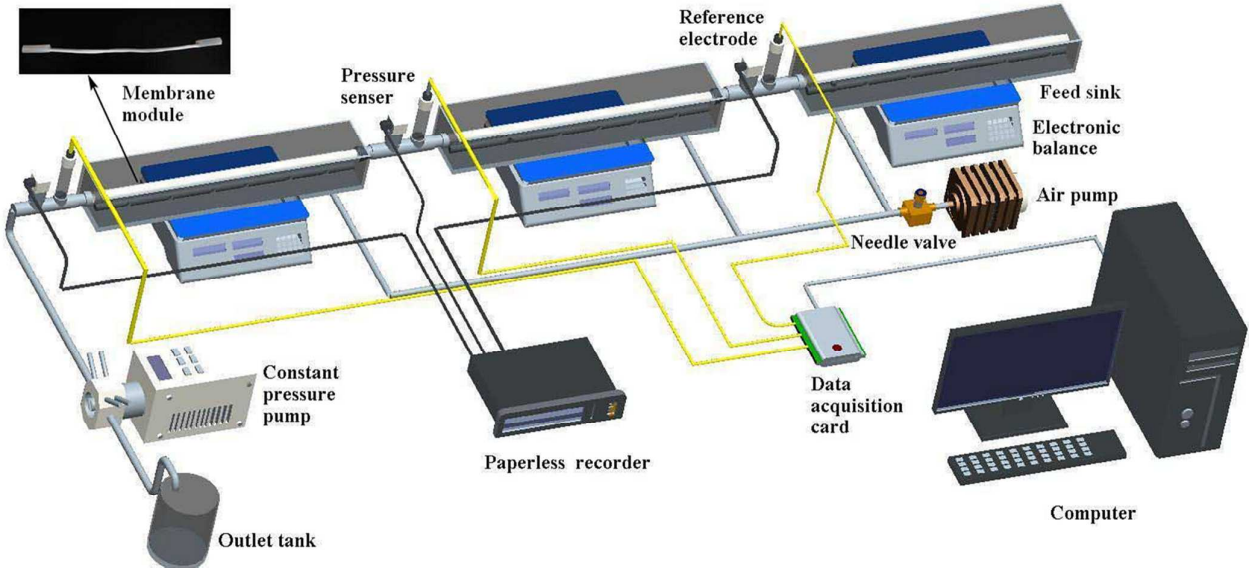

Fig. 2 Experimental apparatus for simultaneously monitoring local flux and zeta potential.

In order to figure out surface charge characterization of yeast solution and clean membrane, the zeta potential of yeast solution and clean membrane under different pH were measured using Zeta-Plus (Zetasizer nano ZS90, Malvern Instruments, UK and PALS, Brookhaven Instruments Corp, USA), respectively.

As shown in Fig. 1, zeta potential of yeast solution and clean membrane changes from positive to negative with the increase of pH. The isoelectric point of yeast solution and clean membrane are around pH 3.8 and 4.2, respectively. pH of yeast solution adopted in this study was 6.1 (yeast solution is prepared directly, without acid and alkali). From Fig. 1, the zeta potential of the yeast solution was -18.5mV, while the clean membrane was -6.1mV. Data show that yeast solution and the surface of membrane pore wall employ a same-charged condition with negative charges at pH of 6.1.

2.2. Simultaneously monitoring local flux and zeta potential systems

The schematic diagram of simultaneously monitoring local flux and zeta potential systems is shown in Fig. 2. Three feed sinks were connected in-series with the membrane module inserted by quick pipe connector. Constant pressure pump (TP 10–20, Motimo, China) was used to drive the constant overall pressure. Three pairs of commercial Ag/AgCl electrodes (218 reference electrode, Shanghai Leici, China) were placed on permeate and retentate sides which were close to the membrane module, respectively.[20] The electrodes were connected to a data acquisition system (USB-FS1208, Measurement ComputingTM, Hungary) which recorded experimental data once every 4 min automatically. The changes of transmembrane pressure (TMP) of three membrane sections were monitored using pressure sensors (Danfoss, MBS 3000, Denmark) which recorded once automatically every 4 min by a paperless recorder (MIK210B, MEACON, China). Integrated data processing software recorded the variation of electronic balance (CN-AS, Taiwan Yinghua, China) which measured the effluent weight once every 4 min and transfered it into membrane flux. It was noteworthy that the liquid levels of three tanks were kept relatively constant manually. Air pump (ACO-818, Sensen Industry Co. Ltd., Zhoushan, China) worked at a certain rate of aeration to prevent the sedimentation of feed suspension. All the experiments repeated at least five times.

2.3. The calculation of the zeta potential

Electrokinetic techniques such as streaming potential measurements have been applied in the characterisation of the surface charge condition of membranes, and the streaming potential can be monitored during filtration. The fundamental relationship between the measured streaming potential and the membrane zeta potential is reasonably given by the well-known Helmholtz–Smoluchowski (H–S) equation (1)[20,21]:

$$\frac{\Delta P}{\Delta E} = \frac{\varepsilon\varepsilon_0\xi}{\mu\lambda} \quad (1)$$

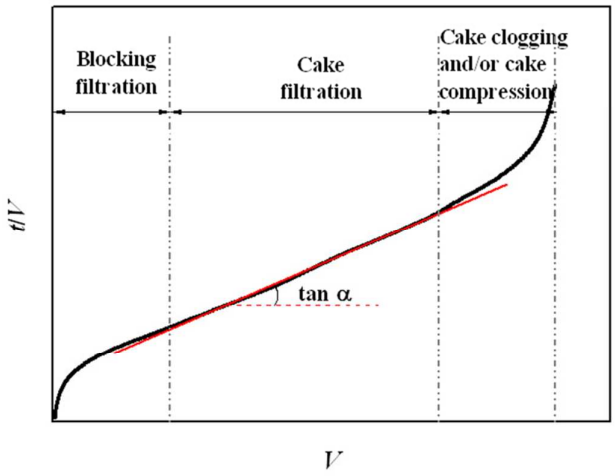

Fig. 3 Ratio of filtration time and volume (t/V) vs. filtrate volume (V).[22]

Where ΔE is the streaming potential difference, mV; ΔP is the transmembrane pressure drop, Pa; ε is the relative dielectric constant of the electrolyte solution; ε_0 is the vacuum dielectric constant, s/m·Ω; ξ is the zeta potential, mV; μ is the solution viscosity, Pa·s; λ is the solution conductivity, 1/m·Ω. The electrolyte solution was 1.0mM KCl. Moreover, Eq. (1) is restricted to the limit of $r_P/\kappa^{-1} > 10$ (r_p is pore radius, m; κ^{-1} is Debye length, m). In this study, $r_P/\kappa^{-1}=22.85 > 10$, Eq. (1) is applicable to calculate the zeta potential.

It should be pointed out that the membrane zeta potential determined from Eq. (1) is an apparent value. This paper put emphasis on the change of zeta potential over time. If need a more rigorous zeta potential, one could consider the corrected H-S equation.[17]

2.4. Fouling model

Plenty of researches have established mathematical models to investigate the forms of membrane fouling [3,4,5,22,23], among them a widely used and simple combined fouling model to analyze flux decline data is t/V vs. V plot, shown in Fig. 3. Where t is filtration time; V is the permeate volume.

The t/V vs. V plot typically shows three regions in membrane filtration which corresponds to (i) blocking filtration, (ii) cake filtration, (iii) cake clogging and/or cake compression. The initial curve depicting a gradual reduction in the slope with increasing V results from a pore blocking mechanism. The linear part characterizes well the filtration mechanism of cake filtration. The final part of the curve which indicates a considerable increase in flow resistance may arise from the formation of a compressible cake or from subsequent clogging of cake flow passages.[22]

3. Results and discussion

3.1. Section characterization of local fouling forms by zeta potential and local flux

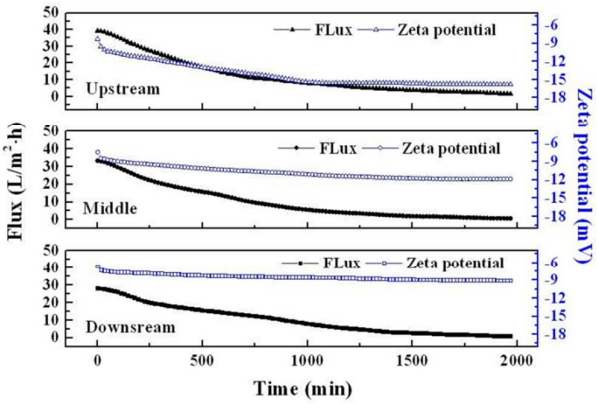

Fig. 4 Flux and zeta potential variations of three parts of membrane module against filtration time at fiber length of 1.2 m and TMP about 0.50 bar.

From the overall point of view, it could be shown in Fig. 4 that both of local flux and zeta potential decrease along the membrane filtration process due to the fouling resistance increases. No matter which part of the membrane (upstream, middle, or downstream) it was, time evolution of the zeta potential was closely related to the filtrate flux decline. The same phenomena were also found by Y. Soffer et al[17] and J.H. Sung et al].[14] Additionally, it could be discovered that zeta potential values vary between clean membrane and yeast solution.

The absolute value of the zeta potential at upstream was larger than another. This might be due that the negatively charged yeast particles hardly deposited onto the outer surface of the negatively charged hollow fiber membrane, in contrast, formed the concentration polarization layer that suspended in the membrane surface. Moreover, uneven driving force and shear force would lead to greater concentration polarization at upstream than that at middle.[20] The feed permeate rate becomes increasing as it goes to the upstream due to the radial permeation, and thus the pressure drop is changed.[24]

As shown in Fig. 4, the zeta potentials of the three sections dropped quickly at the initial a few minutes, then gently declined till the end. The rapid dropped in the zeta potentials at the initial time might be formed pore blocking, it also attributed to the electrostatic repulsion between charged membrane surface and yeast suspension, the formation of double electrode layer as well as concentration polarization. Followed by cake filtration.[25] The formation of cake layer prevented the further blocking of membrane pores, so zeta potential values of three sections tended to be more gentle, it attributed to the weakened electrokinetic flow resulting from the narrowed membrane pores due to the continued deposition of yeast particles. As membrane filtration continued, zeta potential values of three sections appeared to be stable, which might enter cake layer compression stage.

Combining with flux data of three segments, and referring to the model established in Fig. 3, meanwhile contrasting Fig. 3 and Fig. 5(a), it implied that pore blocking occurred in a short period at the beginning of the filtration, then cake formation, following cake compression. Coupled with the zeta potential data in Fig. 5(b), it suggested that the zeta potential rapidly decreased in the early stage of the filtration and then dropped gradually and linearly till almost stable at the end of membrane filtration, which meant that membrane filtration experienced pore blocking, cake filtration and cake compression. The conclusions about pore blocking and cake filtration were consistent with the research of K. Nakamura et al.[25] Nevertheless, they assumed the zeta potential jumped from that of clean membrane to a certain value between it and the cake layer's zeta potential as filtration started and became nearly stable in the pore blocking filtration, followed by the cake filtration. What is more, the existence of cake layer compression has not been taken into account yet.

In the filtering process, the upstream entered into the cake formation and cake compression stage firstly. A period of time entering into the cake formation stage at upstream, middle and downstream were t_{O1}=20min, t_{M1}=22min, t_{E1}=24min, respectively; and into the cake compression stage time points were t_{O2}=1032min, t_{M2}=1112min, t_{E2}=1240min, respectively, when fitting the data of cake formation stage to obtained line-

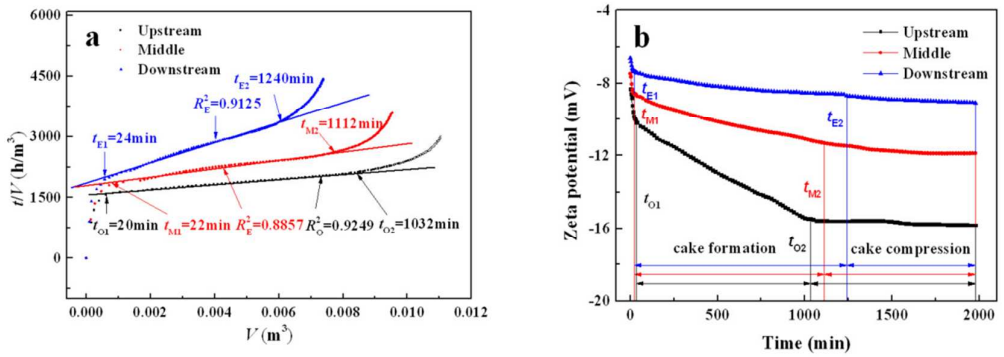

Fig.5 Ratio of t/V vs. V (a) and zeta potential against filtrate time (b) about upstream, middle, downstream at 1.2 m fiber length and TMP about 0.50 bar.

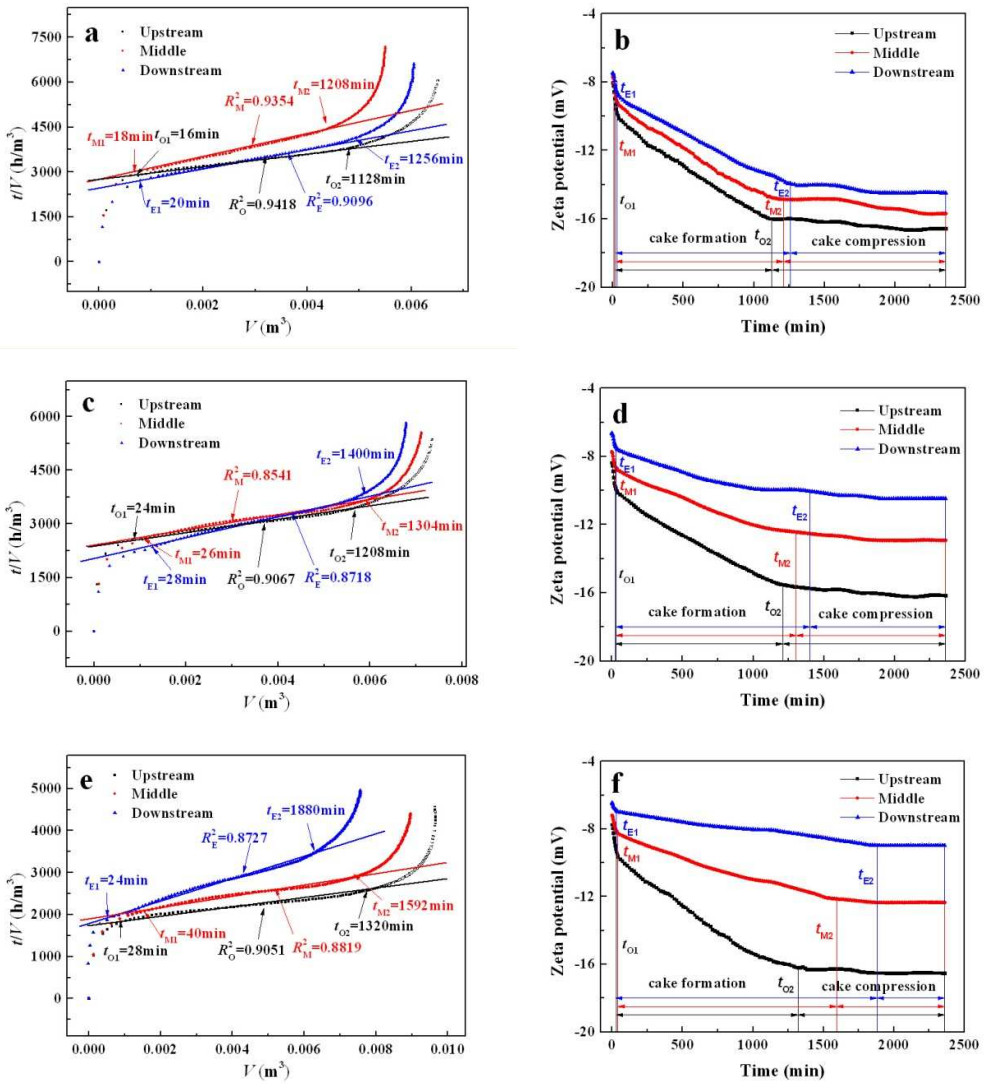

Fig.6 Ratio of t/V vs. V (a, c, e) and zeta potential against filtrate time (b, d, f) in upstream, middle, and downstream parts with different fiber length (0.6m, 1.2m, 1.8m) at about 0.35 bar.

ar equations (R^2_o = 0.9249, R^2_M = 0.9125, R^2_E = 0.8857). And it reflected that cake formation and cake compression of the middle as early as the downstream, because the internal pressure in the fiber lumen dropped from the upstream to the downstream during dead-end hollow fiber membrane filtration process.

3.2. Effect of fiber length on local fouling forms

In the case of a constant TMP 0.35 bar, the local zeta potential variations in different fiber length (0.6, 1.2, 1.8 m) were investigated to study the effect of fiber length on local fouling forms.

As shown in Fig. 6(a) and 6(c), the upstream first entered into cake layer formation stage due to the suction pressure largest near the pump at the condition of dead-end filtration. But when fiber length increased to 1.8m shown in Fig. 6(e), the downstream entered into cake layer formation stage first, because fiber length was so long that the local flux at the downstream decreased very slowly and almost had no change at first, the ratio of t/V vs. V was increased sharply. With fiber length increasing, A period of time entering into the cake compression stage at upstream, middle and downstream were $t_{O2\text{-}0.6}$=1128min, $t_{M2\text{-}0.6}$=1208min, $t_{E2\text{-}0.6}$=1256min, $t_{O2\text{-}1.2}$=1208min, $t_{M2\text{-}1.2}$=1304min, $t_{E2\text{-}1.2}$=1400min, $t_{O2\text{-}1.8}$=1320min, $t_{M2\text{-}1.8}$=1592min, $t_{E2\text{-}1.8}$=1880min, respectively. The time entering into cake compression stage extended obviously as fiber length increased. But no matter how long fiber length was, the upstream first came into cake formation stage. This was because the internal pressure in the fiber lumen dropped from the upstream to the downstream during dead-end hollow fiber membrane filtration process which led to fouling uneven distribution, and it may occurs a fouling redistribution phenomenon.

Compared with the data of zeta potential in Fig. 6(b), (d) and (f), it also could be seen that zeta potential values ranged

between clean membrane and yeast solution. And with the increase of fiber length, the zeta potential difference values of three segments had increasing tendency. The main reason was the uneven hydrodynamic distribution along the fiber including TMP and local flux, leading to uneven distribution of concentration polarization and membrane fouling. According to the fouling uneven theory of hollow fiber membrane[26], fouling resistance increases gradually along the membrane filtration, which results in the local flux uneven distribution. The longer the membrane fiber is, the greater the uneven of local flux performs. Therefore, the zeta potential difference values of three segments tended to increase. The growth of cake layer had indeed slowed with the increase of fiber length, and then a weakened electrokinetic flow owing to a lower permeate flux led to a decrease of the membrane zeta potential.

In sum, zeta potential did reflect the forms of local membrane fouling. When the zeta potential rapidly decreased, pore blocking occured. In the cake filtration, zeta potential declined gradually and linearly, while the zeta potential was almost stable, showing that cake compression was experienced.

4. Conclusions

The responses of zeta potential to local membrane fouling behavior were studied by monitoring both local flux and local zeta potential during dead-end membrane filtration. The forms of zeta potential change during membrane filtration were quite different among pore blocking, cake formation and cake compression processes. Zeta potential was rapidly decreased during pore blocking process; and in the cake formation process zeta potential declined gradually and linearly, while the zeta potential became almost stable as the process of cake compression was experienced.

During the process of dead-end membrane filtration, the zeta potential values ranged between clean membrane and filtration solution. In addition, fiber length had a significant impact on local zeta potential distribution and local membrane fouling forms. With the increase of fiber length, the time of three segments taken for coming into cake compression stage were extended and the zeta potential difference values of three segments tended to increase. It provided new insights in membrane fouling measurement, which could be advantageous for understanding the characteristics of membrane fouling process.

Acknowledgements

This study is financially supported by the National Natural Science Foundation of China (No. 51378349), China Postdoctoral Science Foundation (2013M541184), and Program for Changjiang Scholars and Innovative Research Team in University of Ministry of Education of China (Grand No. IRT13084).

References

1 K.J. Martin, D. Bolster, N. Derlon, E. Morgenroth and R. Nerenberg, *J. Membr. Sci.*, 2014, **471**, 130–137.
2 K.J. Howe and M.M. Clark, *Environ. Sci. Technol.*, 2002, **36**, 3571–3576.
3 L.F. Song, *J. Membr. Sci.*, 1998, **139**, 183-200.
4 T. Mohammadi, M. Kazemimoghadam and M. Saadabadi, *Desalination.*, 2003, **157**, 369–375.
5 G. Bolton, D. LaCasse and R. Kuriyel, *J. Membr. Sci.*, 2006, **277**, 75-84.
6 M.C.V. Vela, S.A. Blanco, J.L. García and E.B. Rodríguez, *Sep. Purif. Technol.*, 2008, **62**, 489–498.
7 J. Shin, K. Kim, J. Kim and S. Lee, *Desalination.*, 2013, **309**, 213–221.
8 C.C. Ho and A.L. Zydney, *J. Colloid Interface Sci.*, 2000, **232**, 389.
9 G. Bolton, D. LaCasse and R. Kuriyel, *J. Membr. Sci.*, 2006, **277**, 75.
10 C. Dreszer, A.D. Wexler, S. Drusová, T. Overdijk, A. Zwijnenburg, H.-C. Flemming, J.C. Kruithof and J.S. Vrouwenvelder, *Water Res.*, 2014, **67**, 243–254.
11 X.H. Li, J.X. Li, J. Wang, H. Wang, B.Q. He, H.W. Zhang, W.S. Guo and H.H. Ngo, *J. Membr. Sci.*, 2014, **453**, 18–26.
12 X.H. Li, J.X. Li, J. Wang H. Wang, Z.Y. Cui, B.Q. He and H.W. Zhang. *J. Membr. Sci.*, 2014, **451**, 226–233.
13 J. Mendret, C. Guigui, P. Schmitz and C. Cabassud, *J. Membr. Sci.*, 2009, **333**, 20-29.
14 J.H. Sung, M.S. Chun and H.J. Choi, *J. Colloid Interface Sci.*, 2003, **264**, 195-202.
15 Z.P. Zhao, Z. Wang and S.C. Wang, *J. Chem Eng Data (China).*, 2003, **54**, 417–418.
16 B.Teychene, P. Loulergue, C. Guigui and C. Cabassud, *J. Membr. Sci.*, 2011, **370**, 45–57.
17 Y. Soffer, J. Gilron and A. Adin, *Desalination.*, 2002, **146**, 115–121.
18 M.S. Chun and W.C. Park, *J. Membr. Sci.*, 2004, **243**, 417–424.
19 S. Schiewer and B. Volesky, *Environ. Sci. Technol.*, 1995, **29**, 3049–3058.
20 Y.R. Qiu and J. Qi. *J. Membr. Sci.*, 2013, **425–426**, 71–76.
21 M. Nystrom, A. Pihlajamaki and N. Ehsani, *J. Membr. Sci.*,1994, **87**, 245–256.
22 S.F.E. Boerlage, M.D. Kennedy, M.P. Aniye, E. Abogrean, Z.S. Tarawneh and J.C. Schippers, *J. Membr. Sci.*, 2003, **211**, 271–289.
23 R. van Reis and A. Zydney, *J. Membr. Sci.*, 2007, **297**, 16–50.
24 M.S. Chun, H.I. Cho and I. K. Song, *Desalination.*, 2002, **148**, 363–367.
25 K. Nakamura, T. Orime and K. Matsumoto, *J. Membr. Sci.*, 2012, **401–402**, 274–281.
26 M.C. Vincent-Vela, E. Bergantiños-Rodríguez, S. Álvarez-Blanco and Lora-García J, *Desalin Water Treat.*, 2009, **10**, 134-138.

